

PAPER • OPEN ACCESS

Discrete-continuous optimisation of an axial flow blood pump

To cite this article: K Tesch and K Kaczorowska-Ditrich 2018 *J. Phys.: Conf. Ser.* **1101** 012044

View the [article online](#) for updates and enhancements.

You may also like

- [Developments in control systems for rotary left ventricular assist devices for heart failure patients: a review](#)
Abdul-Hakeem H AlOmari, Andrey V Savkin, Michael Stevens et al.
- [Non-invasive estimation of pulsatile flow and differential pressure in an implantable rotary blood pump for heart failure patients](#)
A H AlOmari, A V Savkin, D M Karantonis et al.
- [Non-invasive estimation and control of inlet pressure in an implantable rotary blood pump for heart failure patients](#)
A H AlOmari, A V Savkin, P J Ayre et al.

PRIME
PACIFIC RIM MEETING
ON ELECTROCHEMICAL
AND SOLID STATE SCIENCE

HONOLULU, HI
Oct 6-11, 2024

Abstract submission deadline:
April 12, 2024

Learn more and submit!

Joint Meeting of
The Electrochemical Society
•
The Electrochemical Society of Japan
•
Korea Electrochemical Society

Discrete-continuous optimisation of an axial flow blood pump

K Tesch and K Kaczorowska-Ditrich

Gdansk University of Technology, ul. G. Narutowicza 11/12, 80-233 Gdansk, Poland

E-mail: krzyte@pg.edu.pl

Abstract. This paper presents results of discrete-continuous optimisation of an axial flow blood pump. Evolution Strategies (ES) are used as a global optimisation method in order to localise the optimal solution in relatively short time. The whole optimisation process is fully automated. This also applies to geometry modelling. Numerical simulations of the flow inside the pump is performed by means of the Reynolds-Average Navier-Stokes approach. All equations are discretised by means of the finite volume method and the corresponding algebraic equation systems are solved by the open source software for CFD, namely OpenFOAM. Finally, optimisations results are presented and discussed. The objective function to be maximised is simply pressure increase. The higher pressure increase the lower angular velocities required. This makes it possible to minimise the effect of haemolysis because it is mainly caused by high shear stress which are related, among others, to angular velocities.

1. Introduction

Since advanced medical treatment is usually not enough to prevent further decline of patients with heart failure, two treatments of patients with such a disease can be distinguished, namely heart transplantation and artificial heart blood pumps. The former is somewhat difficult because of relatively high costs and, what is even more important, lack of donor organs [5], not to mention organ rejection and mortality rates. The latter approach to heart failure problem, i.e. artificial heart pumps, gain popularity due to constantly improved design and features.

Several design of artificial hearts are know. The most complicated aim to replace the ailing heart whereas simpler pumps are design in order to support it. The supporting devices fall into three groups: LVAD (left ventricular assist device), RVAD (right ventricular assist device) and BIVAD (bi-ventricular assist device) [3]. Despite the fact that the human heart nature is pulsatile, continuous flow pumps are the most popular solutions. This is because of the simplicity reason and size of the device. Furthermore, we can distinguish centrifugal and axial blood pumps. The latter being smaller in comparison with the former. However, axial blood pumps require significantly higher angular velocities in order to increase outlet pressure. This may lead to blood damage, i.e. thrombosis and haemolysis [10, 9, 1] in particular. Haemolysis is mainly caused by high shear stress [2]. In order to minimise the effect of haemolysis an optimisation process of the axial pump is undertaken. The optimisation results leads to improvement in reduction of the wall shear stresses.



2. Geometry description

The whole geometry consists of a rotor and stator and is described by fourteen parameters (design variables) $\mathbf{x} = \{x_1, \dots, x_{14}\}$ listed in table 1. First of all, the rotor blade shape is a non-linear helix given by

$$x(t) = R \cos t, \quad (1)$$

$$y(t) = R \sin t, \quad (2)$$

$$z(t) = f(t) \quad (3)$$

where R stands for the radius of rotor blades. Further, the parameter $t \in [0; 2\pi x_1]$ is related to rotor blade pitch $2\pi x_1$. The non-linearity $f(t)$ of the helix (1) is described by one parameter x_2 shown in figure 1.

Two of fourteen design variables are discrete, i.e. the number of rotor and stator blades. The former is named x_3 and the latter x_8 . Next, the shape of the shaft is described by four points (x_4, x_5) , (x_6, x_7) of the spline shown in figure 1. Stator blades are given by the so called camber line and the blade thickness. The former is represented by two variables (one points) (x_{11}, x_{12}) of the spline whereas the latter by two variables (two points) $(0, x_{13})$, $(1, x_{14})$, see figure 2. Finally, the two remaining variable x_9 and x_{10} are the stator blade upper and lower twist angles, respectively. The considered rotor radius R is 8 mm and the length of the shaft is $4.5 R$.

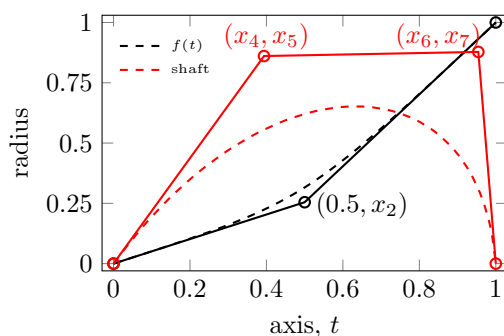


Figure 1. Shaft and helix splines.

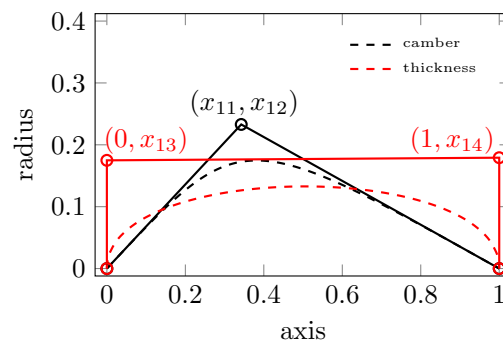


Figure 2. Stator splines.

The whole optimisation process is fully automated. This also applies to geometry modelling.

3. CFD

3.1. Governing equations and discretisation

Numerical simulations of the flow inside the pump is performed by means of the Reynolds-Average Navier-Stokes approach. A closed system of equations [14] for incompressible fluid and two additional transport equation for the two-equation SST [6] model is solved.

All the equations are discretised by means of the finite volume method and the corresponding algebraic equation systems are solved by the open source software for CFD, namely OpenFOAM [8]. Divergence schemes include both convection and other diffusive terms and involve Gauss integration. The discretised convection terms need to be interpolated by means of cell centred values because the values are located at the face centroids. Limited linear interpolation is used, being second order accurate. Further, the discretised diffusive terms involving surface normal gradients are evaluated at a cell face that connects two cells. In order to maintain second order accuracy for non-orthogonal meshes, apart from orthogonal schemes, a non-orthogonal correction is considered.

The SIMPLE algorithm is used in order to solve pressure-velocity coupling and the pressure equation is solved by means of GAMG solver with DIC smoother. For the velocity fields and turbulent quantities standard solvers using a GS smoother are utilised. Under-relaxation factors are used in order to improve stability of a solution. This is particularly important when solving steady-state flows. The assumed factors are 0.3 for pressure, 0.7 for velocity and 0.5 for turbulent quantities k and ω .

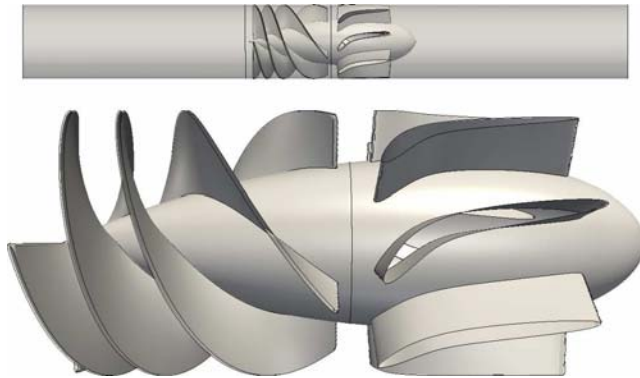


Figure 3. Flow domain (top) and optimal pump geometry (bottom).

3.2. Mesh and boundary conditions

The flow domain is divided into three parts, see figure 3. Apart from the rotating rotor, two additional steady pipes are considered. All three domains are discretised separately and merged by the so called arbitrary mesh interface. The total number of nodes is 1 553 806 and total number of volumes 1 378 033 where 1 269 555 of them are hexahedra. Furthermore, the mesh used may be classified as Cartesian, see figure 4.



Figure 4. Mesh.

In order to make certain that flow near walls is properly resolved thin layers around the physical walls are generated. The quality of the mesh near the walls is inspected in terms of the maximal y^+ values. Maximal values of y^+ are below 3 for all considered walls including blades.

The main boundary conditions are:

- Inlet. The specified constant volumetric flow rate $\dot{V} = 3 \text{ dm}^3/\text{min}$ is directed perpendicularly to inlet surface accompanied by the zero normal gradient pressure. Low turbulence intensity is also considered. This means that turbulence intensity is at the level of 1% and viscosity ration $\nu_t/\nu = 1$;
- Outlet. The constant pressure distribution is assumed here together with zero gradient velocity for flow out of the domain. This is because the outlet surface is located relatively far from the rotor;

- Walls. The so called no-slip conditions is applied meaning that impermeability and adhesion requirements are forced. Rotating wall velocity $n = 6000$ rev/min is considered in the rotating frame of reference. The flow in the near wall region is modelled by means of the scalable wall function;
- Interfaces. In order to allow for coupling between stationary pipes and rotating part of the pump the so called cyclic arbitrary mesh interfaces are considered. A steady state approach is used rather than full transient rotor-stator interaction. This is crucial for time consuming optimisation processes since CFD calculations need to be repeated hundred of times. This approach is commonly known as a multiple reference frame simulation;

4. Optimisation

4.1. General remarks

A discrete-continuous optimisation approach is needed to find the optimal shape. This is because two of fourteen design variables are discrete, namely the number of rotor and stator blades. Remaining variables such as the shaft, rotor and stator shapes as well as their thickness are continuous.

Evolution Strategies are used as a global optimisation method to localise the optimal solution in relatively short time [7, 11]. ES can be further classified as multi-point (population based) optimisation algorithms. Recombination, mutation and survival are adapted in order to evolve better solution. Most importantly, no additional information about the objective function is required. Additionally, randomisation is introduced through the probability of crossover and mutation. This makes it possible to efficiently explore the design space and escape local minima.

4.2. Objective function

The optimisation problem is to find a maximal pressure increase Δp . Since most optimisation algorithms are designed for minimisation of objective function, the pressure increase is considered with a minus sign

$$\Delta p_0 = \min_{\mathbf{x} \in \Omega \subseteq \mathbb{R}^D} (-\Delta p(\mathbf{x})). \quad (4)$$

Furthermore, the argument of the global minimum value of the objective function is expressed as

$$\mathbf{g} = \arg \min_{\mathbf{x} \in \Omega \subseteq \mathbb{R}^D} (-\Delta p(\mathbf{x})) \quad (5)$$

where $D = 14$ stands for the dimension of constraint space Ω or simply the so called optimisation domain. Thus, the objective function is subjected to box constraints listed in table 1

$$\Omega = \{\mathbf{x} \in \mathbb{R}^D : L_i \leq x_i \leq U_i\} \quad (6)$$

where L_i and U_i are lower and upper bounds, respectively. Box constraints are regarded as a special case of inequality constraints. This type of constraints is commonly met in optimisation problems and does not need any special treatment.

4.3. Algorithm

The ES algorithm in the pseudocode from [11] is shown in figure 5. Firstly, the initial population is randomly generated by means of a random variate of a continuous uniform distribution (lines 1-3). Lines 7 and 8 represent parent selection steps. This is achieved by means of tournament selection (lines 7 and 8) where $T = 3$ stands for the tournament size out of a parent population of N members. Once parents are selected, the arithmetical crossover is performed (line 11).

Input: $p_c, p_m, T, N, n_{max}, \mathbf{L}, \mathbf{U}$
Output: \mathbf{g}

```

1 for  $i := 0$  to  $N - 1$  do
2    $\mathbf{x}_i := \mathbf{L} + (\mathbf{U} - \mathbf{L}) \circ \mathcal{U}(0, 1)$ ;
3    $\mathbf{y}_i := \mathbf{0}$ ;
4    $\mathbf{g} := \arg \min_{\mathbf{x}_i} f(\mathbf{x}_i)$ ;
5   for  $n := 1$  to  $n_{max} - 1$  do
6     for  $i := 1$  to  $N - 1$  do
7        $a := \text{Tournament}(\mathbf{x}, T)$ ;
8        $b := \text{Tournament}(\mathbf{x}, T)$ ;
9        $\mathbf{p}_1 := \mathbf{x}_a$ ;
10       $\mathbf{p}_2 := \mathbf{x}_b$ ;
11       $(\mathbf{c}_1, \mathbf{c}_2) := \text{Crossover}(\mathbf{p}_1, \mathbf{p}_2, p_c)$ ;
12       $\mathbf{y}_i := \text{Mutation}(\mathbf{c}_1, i, p_m)$ ;
13       $\mathbf{y}_{i+1} := \text{Mutation}(\mathbf{c}_2, i, p_m)$ ;
14       $i := i + 2$ ;
15    $\mathbf{l} := \arg \min_{\mathbf{x}_i} f(\mathbf{x}_i)$ ;
16    $\mathbf{g} := \arg \min \{f(\mathbf{g}), f(\mathbf{l})\}$ ;
17    $\mathbf{x} = \text{Selection}(\mathbf{x}, \mathbf{y})$ ;

```

Figure 5. Evolutionary strategy pseudocode.

Namely, two parents \mathbf{x}_1 and \mathbf{x}_2 are crossed with probability p_c . Two offspring vectors \mathbf{y}_1 and \mathbf{y}_2 are produced according to

$$\mathbf{y}_1 := a \mathbf{x}_1 + (1 - a) \mathbf{x}_2, \quad (7a)$$

$$\mathbf{y}_2 := a \mathbf{x}_2 + (1 - a) \mathbf{x}_1 \quad (7b)$$

where $a := \mathcal{U}(0, 1)$. Next, the integer variables (the number of rotor and stator blades) are uniformly mutated (lines 12-13) if $\mathcal{U}(0, 1) < p_m$ as opposed to floating point variables. The latter are non-uniformly mutated if $\mathcal{U}(0, 1) < p_m$ according to

$$x_{ik} := \begin{cases} x_{ik} + (U_k - x_{ik}) \Delta, & \text{if } \mathcal{U}\{0, 1\} = 0; \\ x_{ik} - (x_{ik} - L_k) \Delta, & \text{otherwise} \end{cases} \quad (8)$$

where

$$\Delta := 1 - \mathcal{U}(0, 1) \left(1 - \frac{n}{n_{max}}\right)^2. \quad (9)$$

In order to damp mutation as the algorithm approaches to an end the value of Δ should decrease.

The selection step (line 17) passes best solutions onto next generations. The so called $(\mu + \lambda)$ strategy is taken into consideration. Here μ denotes the total number of parent vectors \mathbf{x}_i whereas λ is the number of offspring vectors \mathbf{y}_i . In this case $\mu = \lambda = N$. Simply, the considered strategy creates the next parent vector generation with the best μ vectors from the combined $(\mu + \lambda)$ parent and offspring population.

4.4. Results

The EA population size was set as $N = 20$ and the number of generations as $n_{max} = 20$. This results in 400 CFD calculations. Convergence is easily achieved after about 10 generations, see figure 6. The dashed line denotes the average pressure increase for the entire population, while solid line is the global maximum for the entire optimisation process.

Figure 7 shows how the mutation and the crossovers count varies during the optimisation process for the probabilities $p_m = 0.7$ and $p_c = 0.15$. Moreover, figure 8 makes it possible to monitor the population variability as the so called discrepancy is such a measure [13, 12]. Discrepancy D^* takes on values in the neighbourhood of 0 for random populations and close to 1 for uniform populations.

Table 1. Constraints of variables and optimal values.

Name	Constraints	Optimum	Description
x_1	[0.2; 1]	0.823	rotor blade pitch
x_2	[0.1; 0.5]	0.254	non-linearity of the helix
x_3	{2, ..., 4}	4	number of rotor blades
x_4	[0; 0.5]	0.393	two points of shaft's spline
x_5	[0.7; 1]	0.860	
x_6	[0.7; 1]	0.954	
x_7	[0.7; 1.2]	0.877	
x_8	{4, ..., 8}	8	number of stator blades
x_9	[0; 45°]	31.99°	stator blade upper twist angle
x_{10}	[0; 30°]	15.26°	stator blade lower twist angle
x_{11}	[0.2; 0.6]	0.342	point of stator shape blade spline
x_{12}	[0; 0.3]	0.232	
x_{13}	[0.05; 0.3]	0.174	point of stator thickness blade spline
x_{14}	[0.05; 0.2]	0.179	

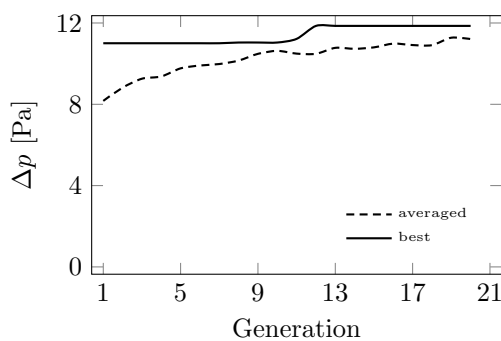


Figure 6. Convergence.

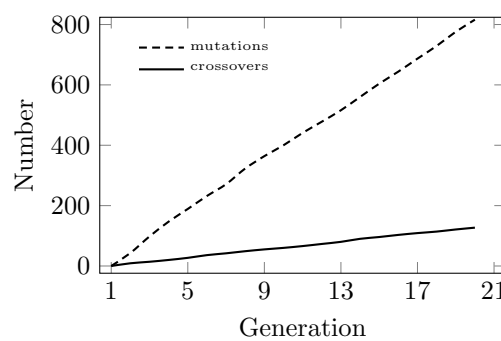


Figure 7. Mutations and crossovers.

The optimal values of \mathbf{g} are listed in table 1. Lower part of figure 3 presents the optimal pump shape according to table 1. It may be observed that the optimal geometry consists of 4 rotor blades and 8 stator blades being the upper accessible ranges. As for the remaining variables, they are located inside the considered box constraints.

The average shape evolution for selected generations (iterations) of ES, reflecting convergence process, is presented in figure 9. It is interesting that the first shape (iteration 1) is simply an arithmetical average of purely random shapes. This is because the initial population is randomly generated. At the same time, the last shape (iteration 20) is similar to the optimal shape since

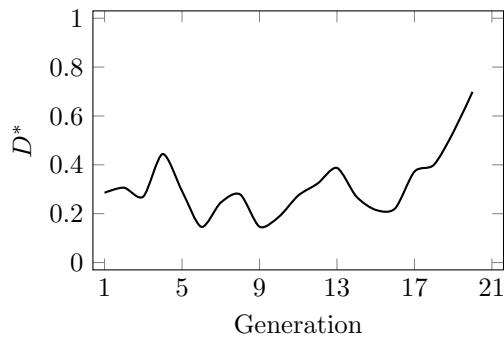


Figure 8. Discrepancy D^* .

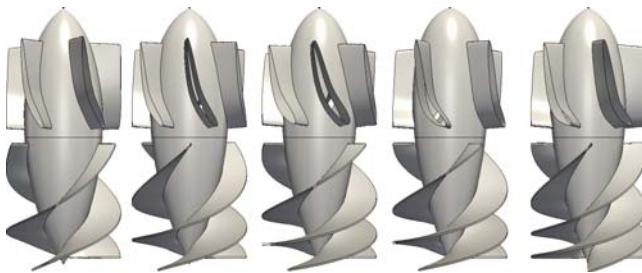


Figure 9. Average shape evolution (iteration number 1, 3, 5, 10 and 20).

the population here is nearly uniform according to the discrepancy value, see figure 8. Finally, since these shapes are arithmetical averages of individual generations, it should be noted that none of these has been subject to any CFD calculations.

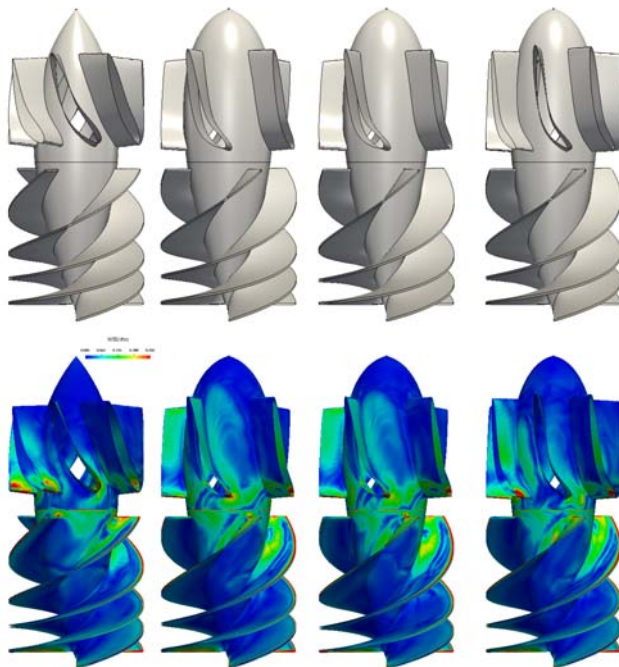


Figure 10. Best shape evolution and corresponding wall shear stresses distributions (iteration number 7, 10, 11 and 20).

Upper part of figure 10 displays the best shape evolution resulting from the shape optimisation process. The last shape (iteration 20) is the optimal solution shown also in figure 3. Interestingly, all shapes apart from first (iteration 7) are similar in terms of rotor configurations. What distinguishes the first geometry from the remaining three is the shape of the shaft and stator

blades. Lower part of figure 10 presents corresponding wall shear stresses distributions. The higher the iteration number the smoother the distribution on the shaft and blades. One has to keep in mind, however, that high shear stresses are related primarily to angular velocities.

5. Conclusions

- Results of a discrete-continuous global optimisation process of an axial flow blood pump are presented. The optimal results are achieved by means of ES in relatively short time. Since 2 of 14 design variables are discrete (integer) special care of ES is necessary;
- A simple and effective method of geometry modelling is proposed. This makes it possible to make the whole optimisation process fully automated. There is no need for any intermediate CAD software since the geometry is created directly by means of GNU Octave [4] scripts;
- Figure 10 presents the wall shear stress distribution which is responsible for haemolysis. It may be observed that the highest values are localised, among other, on the rotor blade tips. The higher pressure increase the lower angular velocity required. Thus the optimisation process leads to improvement in reduction of the wall shear stresses and the effect of haemolysis. This is because haemolysis is mainly caused by high shear stress which are related, among others, to angular velocities;

References

- [1] Aaronson K D et al. 2012 Use of an intrapericardial, continuous-flow, centrifugal pump in patients awaiting heart transplantation *Circulation* **125**(25) 3191
- [2] Behbahani M et al. 2009 A review of computational fluid dynamics analysis of blood pumps *Euro. J. of Applied Mathematics* **20**(4) 363
- [3] Carr C M et al. 2010 CT of Left Ventricular Assist Devices *RadioGraphics* **30**(2) 429
- [4] Eaton J W et al. 2017 GNU Octave version 4.2.1 manual: a high-level interactive language for numerical computations, <https://www.gnu.org/software/octave/doc/v4.2.1/>
- [5] Kafagy D and Gitano-Briggs H 2013 Design of axial blood pumps for patients with dysfunctional fontan physiology: computational studies and performance testing *Trends Biomater. Artif. Organs* **27**(3) 124
- [6] Menter F R 1994 Two-equations eddy-viscosity turbulence models for engineering applications *AIAA-Journal* **32**(8)
- [7] Michalewicz Z 1996 Genetic algorithms + data structures = evolution programs (Berlin, Heidelberg, New York: Springer)
- [8] OpenFOAM user guide 2015, OpenFOAM Foundation Ltd.
- [9] Rogers J et al. 2017 Intrapericardial left ventricular assist device for advanced heart failure *N Engl J Med* **376** 451
- [10] Slaughter M et al. 2013 HeartWare ventricular assist system for bridge to transplant: combined results of the bridge to transplant and continued access protocol trial *J Heart Lung Transpl* **32**(7) 675
- [11] Tesch K 2016 *Continuous Optimisation Algorithms* (Gdansk: GUT Publishers)
- [12] Tesch K and Kaczorowska K 2016 Arterial cannula shape optimization by means of the rotational firefly algorithm *Engineering Optimization* **48**(3) 497
- [13] Thiémond E 2001 An algorithm to compute bounds for the star discrepancy *Journal of Complexity* **17** 850
- [14] Wilcox D C 1994 Turbulence modeling for CFD (California: DCW Industries)